The Shared Genetic Basis of Human Fluid Intelligence and Brain Morphology

Tian Ge[a,b,c,d], Chia-Yen Chen[a,b,d,e], Richard Vettermann[b,c], Lauri J. Tuominen[b,c], Daphne J. Holt[b,c], Mert R. Sabuncu[c,f], Jordan W. Smoller[a,b,d]

[a]Psychiatric and Neurodevelopmental Genetics Unit, Center for Genomic Medicine, Massachusetts General Hospital, Boston, MA 02114, USA; [b]Department of Psychiatry, Massachusetts General Hospital, Harvard Medical School, Boston, MA 02114, USA; [c]Athinoula A. Martinos Center for Biomedical Imaging, Massachusetts General Hospital, Charlestown, MA 02129, USA; [d]Stanley Center for Psychiatric Research, Broad Institute of MIT and Harvard, Cambridge, MA 02138, USA; [e]Analytic and Translational Genetics Unit, Center for Genomic Medicine, Massachusetts General Hospital, Boston, MA 02114, USA; [f]School of Electrical and Computer Engineering and Nancy E. and Peter C. Meinig School of Biomedical Engineering, Cornell University, Ithaca, NY 14853, USA.

Correspondence to Tian Ge

Email: tge1@mgh.harvard.edu

Abstract

Human intelligence differences are linked to diverse cognitive abilities and predict important life outcomes. Here we investigate the biological bases of fluid intelligence in a large sample of participants from the UK Biobank. We explore the genetic underpinnings of fluid intelligence via genome-wide association analysis ($N = 108,147$), and examine brain morphological correlates of fluid intelligence ($N = 7,485$). Importantly, we develop novel statistical methods that enable high-dimensional co-heritability analysis, and compute high-resolution surface maps for the co-heritability and genetic correlations between fluid intelligence and cortical thickness measurements. Our analyses reveal the genetic overlap between fluid intelligence and brain morphology in predominately left inferior precentral gyrus, pars opercularis, superior temporal cortex, supramarginal gyrus, and their proximal regions. These results suggest a shared genetic basis between fluid intelligence and Broca's speech and Wernicke's language areas and motor regions, and may contribute to our understanding of the biological substrate of human fluid intelligence.

Introduction

Human intelligence influences diverse cognitive abilities [1]. Individual differences in intelligence are predictive of important life outcomes, including socioeconomic status, education, job performance, and health and life span [2]. Reductions in intelligence have been associated with numerous psychiatric disorders [3]. Dissecting the biological bases of intelligence, such as its genetic underpinnings and neural correlates, may thus contribute to our understanding of cognitive impairment and related mental illnesses [4].

Twin and family studies have established that human intelligence is substantially heritable [5]. Recent large-scale genome-wide meta-analyses have identified over 200 distinct genomic loci that contribute to individual intelligence differences, and confirmed that intelligence is a highly polygenic trait [6, 7]. In addition, intelligence has shared genetic underpinnings with several neuropsychiatric disorders (e.g., schizophrenia and depressive symptoms) and neurological diseases (e.g., Alzheimer's disease), and has strong positive genetic correlation with educational attainment and longevity [6, 7]. However, the functional consequences of the associated genetic variants have yet to be characterized.

Neuroimaging has been used to examine the relationships between intelligence and brain structure *in vivo* [8]. Higher intelligence has been associated with larger brain size [9–11], and greater total and regional gray matter volumes [12–17]. Positive correlations have been reported between intelligence and cortical thickness measurements primarily in the prefrontal and temporal cortices [18–21]. Overall, structural neuroimaging studies have mapped individual intelligence differences to morphological variation in multimodal association regions. Notably, the parieto-frontal integration theory of intelligence (P-FIT) posits that a network of distributed brain regions may be integrated to process sensory information and support cognitive tasks [22, 23]. However, most prior work on neuroanatomical correlates of intelligence had limited sample sizes, and the shared genetic basis between intelligence and brain morphology remains largely unexplored, outside a small number of investigations with limited spatial resolution [24–27].

In this study, we investigate the genetic and morphological bases of human intelligence using fluid intelligence scores, structural brain MRI scans and genomic data collected by the UK Biobank (`http://www.ukbiobank.ac.uk`) [28]. Fluid intelligence is the capability to reason and solve novel problems independent of any acquired knowledge or experience from the past [29]. It is a factor of general intelligence [30], which is considered the common core shared by all cognitive tests and does not depend on the specific cognitive batteries from which it is constructed [1, 31]. Though a more specialized aspect of cognitive ability, fluid intelligence is known to be highly correlated with general intelligence [4], and is often combined with general

intelligence measurements across cohorts in neuroimaging and genetic studies. Here we first perform genome-wide association analysis of the fluid intelligence score ($N = 108,147$), and calculate its vertex-wise cortical thickness correlates ($N = 7,485$) in the UK Biobank. We then develop a novel statistical method to compute vertex-wise SNP co-heritability and genetic correlations between fluid intelligence and cortical thickness measurements, and localize their shared genetic origins on the cortical surface. SNP co-heritability (genetic correlation) measures the covariance of two traits attributable to common genetic variants, normalized by total phenotypic (genetic) variation. Well-established co-heritability/genetic correlation estimation methods such as genome-wide complex trait analysis (GCTA; also known as the GREML method) [32] and LD (linkage disequilibrium) score regression [33] require either individual genotypes or GWAS summary statistics for the two traits. However, to examine the genetic overlap between a trait whose GWAS summary statistics can be obtained (e.g., a cognitive, behavioral or disease phenotype), and a large number of MRI-derived phenotypes (e.g., fine-grained brain morphological measurements) — a scenario often encountered in imaging genetic studies — both GCTA and LD score regression can be computationally intractable. The proposed method fills this technical gap, and enables high-dimensional co-heritability and genetic correlation estimation, as well as flexible nonparametric statistical inferences. Our analyses expand the literature on the genetic underpinnings and brain morphological correlates of intelligence, construct high-resolution surface maps of co-heritability between fluid intelligence and cortical thickness measurements to unveil their shared genetic basis, and may contribute to our understanding of the biological substrate of human intelligence differences.

Results

GWAS of fluid intelligence. We performed a genome-wide association analysis of the fluid intelligence score derived from the touch-screen questionnaire at the baseline assessment visit in a total of 108,147 unrelated UK Biobank participants of white British ancestry and 7,658,275 genetic variants across the genome that passed quality control (see Methods). Age, sex, age^2, age$\times$sex, age$^2\times$sex, genotype array, UK Biobank assessment center, and top 10 principal components (PCs) of the genotype data were adjusted in the linear regression. We identified 35 independent genome-wide significant regions that were associated with individual fluid intelligence differences (Supplementary Figure S1). Figure 1 shows the Manhattan plot for the GWAS. Using LD score regression [34], the heritability of fluid intelligence captured by common genetic variants (SNP heritability) was estimated to be 0.247 (s.e. 0.008).

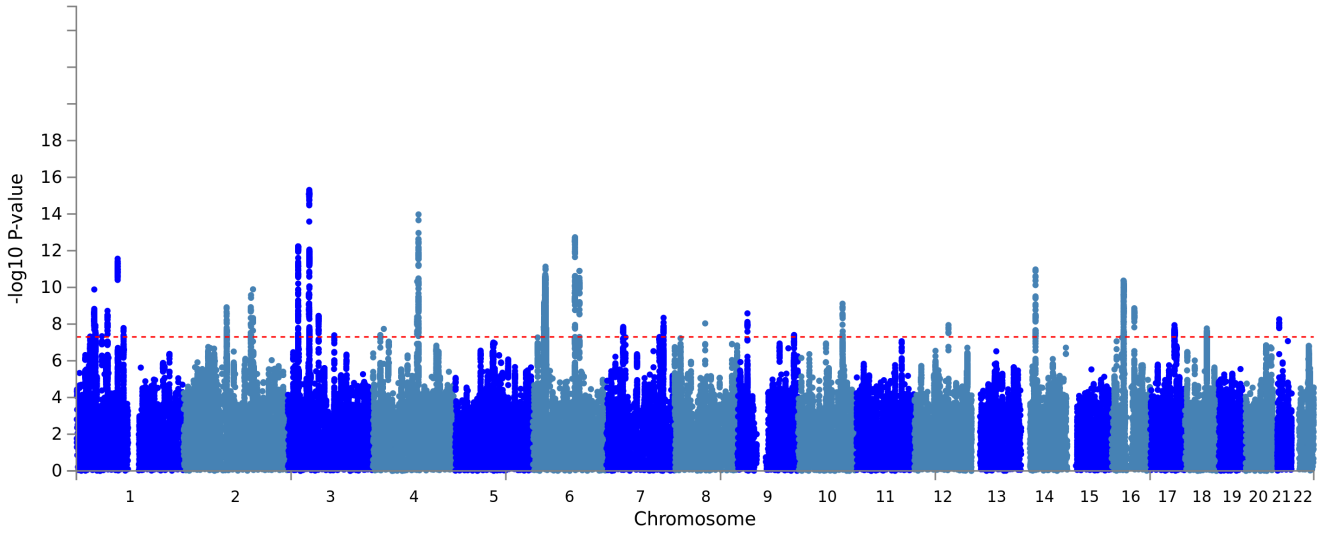

Figure 1: Manhattan plot for the genome-wide association analysis of the fluid intelligence score in the UK Biobank ($N = 108,147$). The dash line indicates the genome-wide significant threshold $p < 5 \times 10^{-8}$.

Cortical thickness correlates of fluid intelligence. Next, we computed Pearson correlations between the fluid intelligence score and vertex-wise cortical thickness measurements, adjusting for age, sex, age^2, age$\times$sex, age$^2\times$sex, in 7,485 participants who had brain MRI scans and intelligence scores collected at the imaging visit. As shown in Figure 2A, higher fluid intelligence was associated with increased cortical thickness in somatomotor cortex, inferior frontal gyrus, inferior parietal lobule, and superior temporal cortex, and reduced cortical thickness in the cingulate gyrus and occipital lobe. More specifically, significant positive correlations between fluid intelligence and cortical thickness measurements were observed in the pars opercularis, supramarginal gyrus and superior temporal gyrus in both hemispheres (Figure 2B).

Heritability of vertex-wise cortical thickness measurements. We estimated the SNP heritability of vertex-wise cortical thickness measurements using an unbiased and computationally efficient moment-matching method described previously [35], in 7,818 participants controlling for age, sex, age^2, age$\times$sex, age$^2\times$sex, genotype array, and top 10 PCs of the genotype data. As an empirical justification, our method produced virtually identical heritability estimates to LD score regression when applied to the average cortical thickness measurements in 68 regions of interest (ROIs; 34 ROIs per hemisphere) defined by the Desikan-Killiany atlas [36] (Supplementary Figure S2, left; also see Methods and *Supplementary Information* for a theoretical treatment). As shown in Figure 3, fine-grained cortical thickness measurements were moderately heritable across

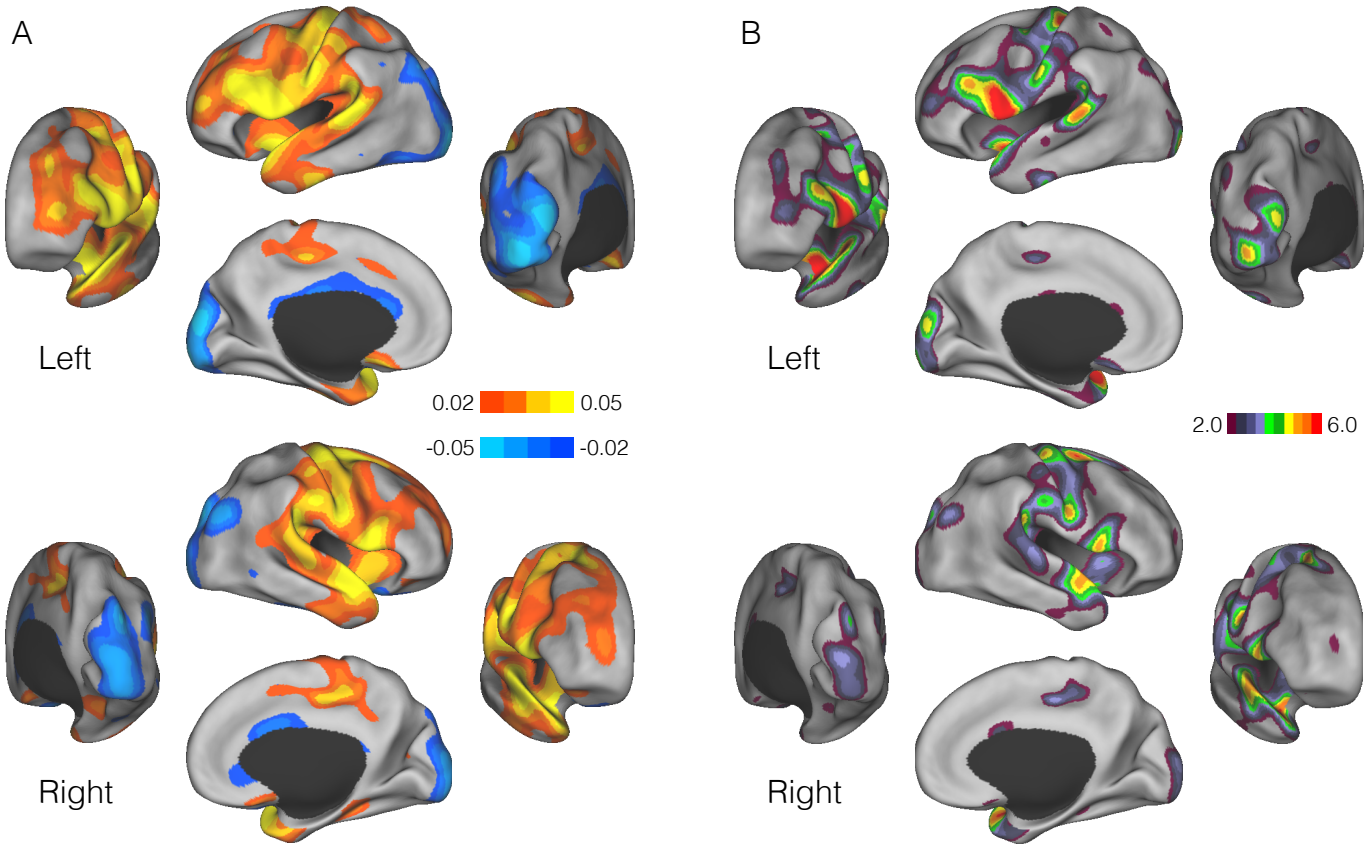

Figure 2: Vertex-wise Pearson correlations between the fluid intelligence score and cortical thickness measurements ($N = 7,485$). (A) Surface maps for the Pearson correlations, adjusting for age, sex, age^2, age$\times$sex, age$^2\times$sex. (B) Surface maps for the $-\log_{10} p$-values of the Pearson correlations.

the cortical mantle.

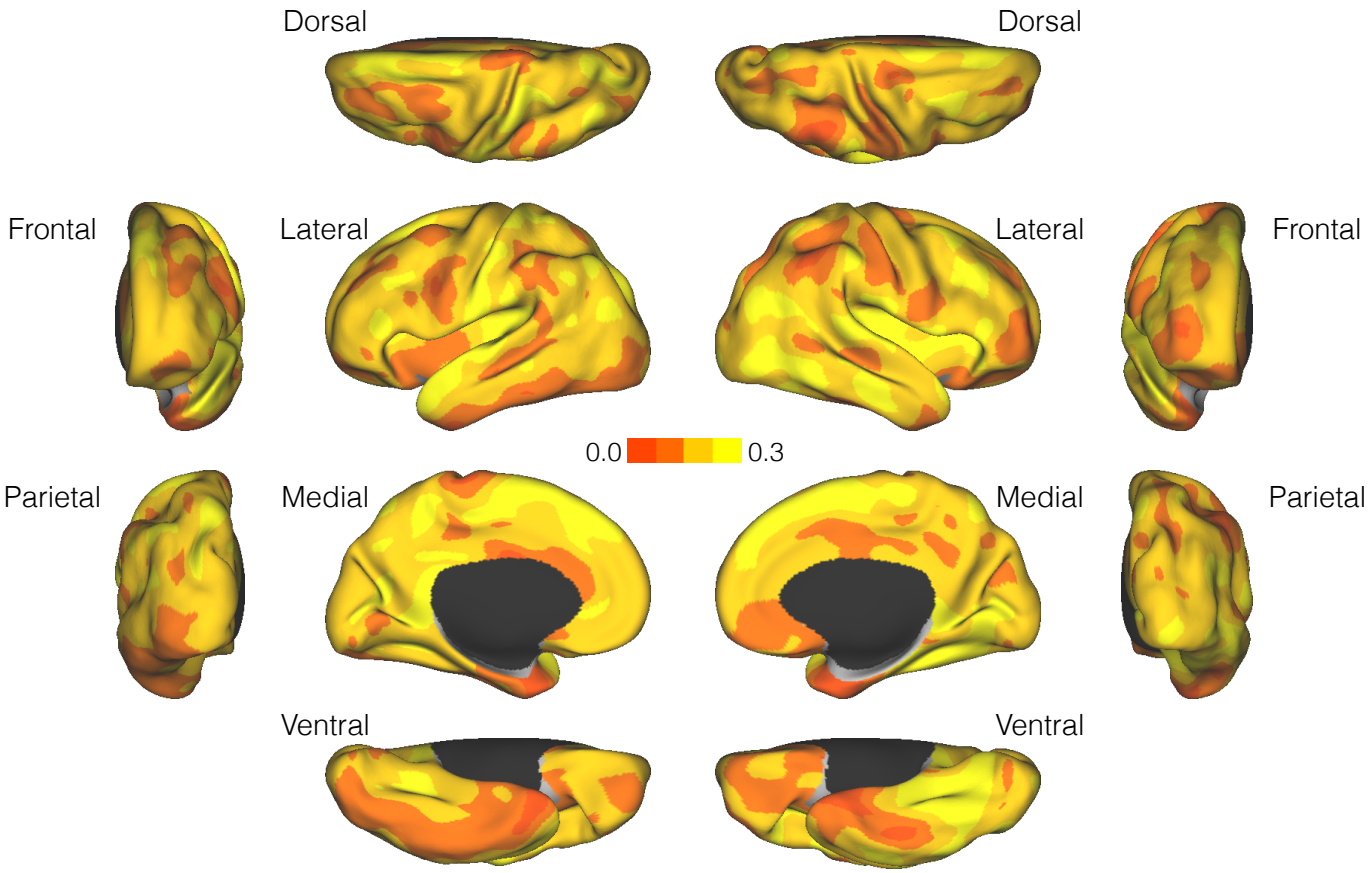

Figure 3: Surface maps for the SNP heritability of cortical thickness measurements ($N = 7,818$).

Co-heritability between fluid intelligence and cortical thickness. Given that fluid intelligence and cortical thickness measurements were both heritable and showed correlations in several brain regions, we sought to examine whether they have a shared genetic basis. Existing methods for co-heritability or genetic correlation estimation are challenging to apply here due to the high-dimensionality of the brain morphological measurements (approximately 300,000 vertices across the two hemispheres). For example, one would have to run hundreds of thousands of GWAS in order to use LD score regression. We developed a novel and computationally efficient method that can leverage the summary statistics of the fluid intelligence GWAS and the individual genotypes of the neuroimaging sample to compute the co-heritability between fluid intelligence and vertex-wise cortical thickness measurements (see Methods). We note that there was no overlap between

the GWAS sample and the imaging sample, which protected our co-heritability estimates from potential bias induced by sample overlap. An empirical comparison of the co-heritability between fluid intelligence and the average cortical thickness measurement in each of the 68 Desikan-Killiany ROIs estimated by the proposed method and LD score regression showed that the two methods produced almost identical estimates (Supplementary Figure S2, right). Theoretical equivalence between the two methods is established in Methods and *Supplementary Information*.

Figure 4A and 4B show surface maps for the co-heritability and its statistical significance between the fluid intelligence score and cortical thickness measurements, respectively, adjusting for age, sex, age^2, age$\times$sex, age$^2\times$sex, genotype array, and top 10 PCs of the genotype data. Unlike the phenotypic correlations, which were largely bilaterally symmetric as shown in Figure 2, the co-heritability between fluid intelligence and cortical thickness showed a predominantly left-hemispheric pattern. We thresholded the significance map using $p = 0.01$ as the threshold (Figure 4B), and assessed the significance of the size of each identified cluster (spatially contiguous vertices) and computed their family-wise error (FWE) corrected p-values using a permutation procedure we devised (see Methods). Positive co-heritability was observed in the left inferior precentral gyrus (cluster 1; $p_{\text{FWE}} = 0.028$), left pars opercularis (cluster 2; also known as Brodmann area 44 or BA44, which is part of the Broca's speech area; $p_{\text{FWE}} = 0.057$), and in cluster 3 ($p_{\text{FWE}} = 0.004$), which spanned the entire superior temporal cortex (including BA22) and extended into the angular gyrus (BA39) and supramarginal gyrus (BA40), a region that overlaps with Wernicke's language area. We did not identify any significant cluster on the right hemisphere ($p_{\text{FWE}} > 0.10$). Supplementary Figure S3 shows the surface map for the genetic correlations between fluid intelligence and cortical thickness measurements, which exhibited a similar pattern to the co-heritability map.

Discussion

In this paper, we investigated the biological bases of human fluid intelligence using large-scale brain imaging and genomic data in the UK Biobank. Specifically, we explored the genetic underpinnings of fluid intelligence via genome-wide association analysis, examined the brain morphological correlates of fluid intelligence, and, more importantly, developed novel statistical methods to map the shared genetic basis of intelligence and fine-grained cortical thickness measurements on the cortical surface. We now discuss each of these advances and the limitations of our analyses below.

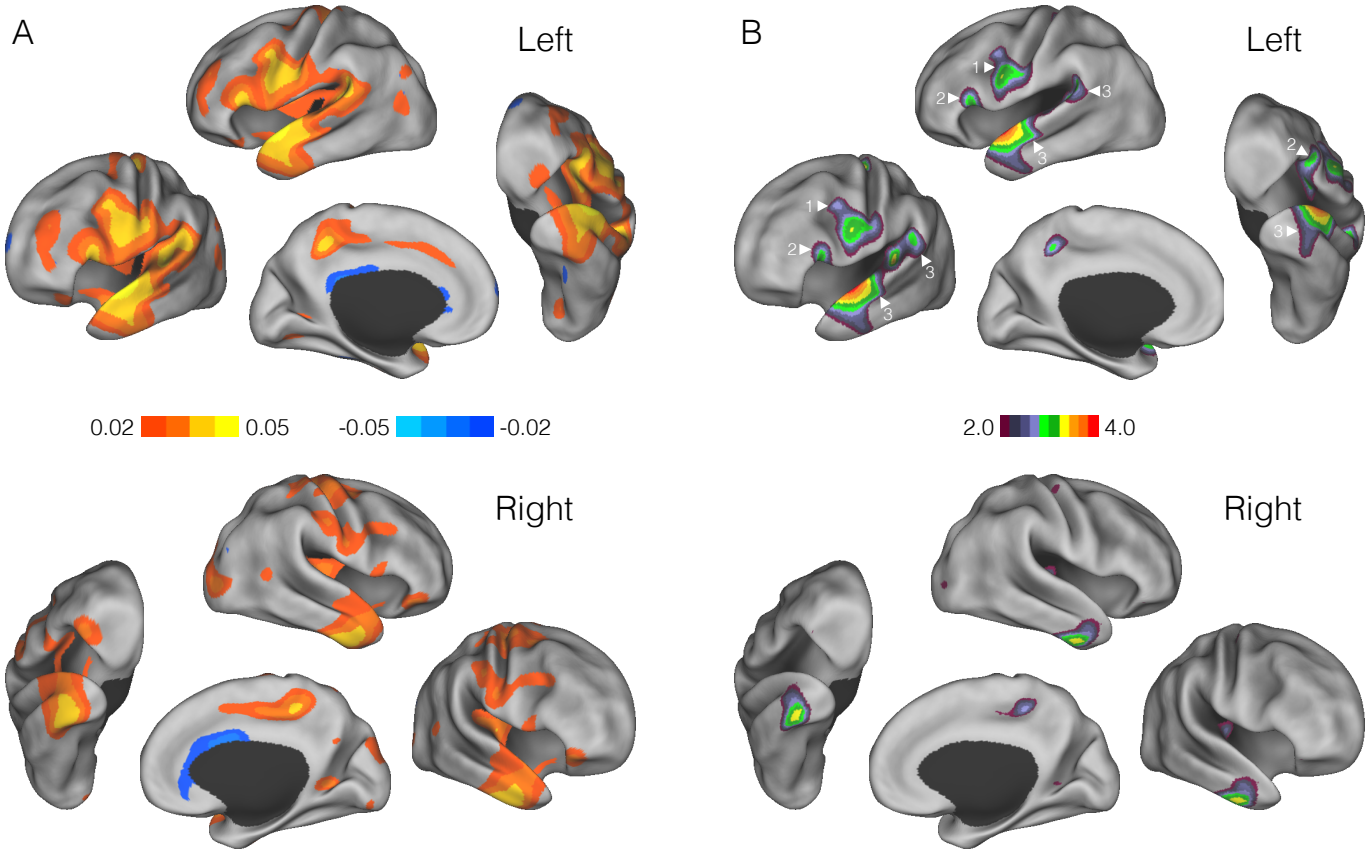

Figure 4: Vertex-wise SNP co-heritability between the fluid intelligence score and cortical thickness measurements. (A) Surface maps for the SNP co-heritability estimates. (B) Surface maps for the $-\log_{10} p$-values of the SNP co-heritability. Clusters identified by a cluster-forming threshold of $p = 0.01$ are shown. Family-wise error corrected significant (or marginally significant) clusters are annotated.

Our genome-wide association analysis of the fluid intelligence score identified 35 independent genomic loci and confirmed the polygenicity and substantial heritability of human intelligence. Previous studies have conducted genome-wide meta-analysis of general intelligence [6, 7, 37], and GWAS with a larger total sample size than the present study exists [7]. Although we could have leveraged the summary statistics of existing GWAS in our co-heritability analysis, we performed our own GWAS in the UK Biobank primarily for two reasons. First, we excluded all participants that had neuroimaging data from our GWAS to ensure that the co-heritability and genetic correlation estimates between fluid intelligence and imaging measurements were not biased by sample overlap. Second, prior genetic analyses of human intelligence often combined various cognitive tests across cohorts to produce a measurement of general intelligence (known as g) [30], while in this study we focused on fluid intelligence, which, together with crystallized intelligence are two specific components of general intelligence [29]. Although it is known that cognitive tests are universally correlated and general intelligence is the common core of cognitive ability, each individual cognitive test also captures substantial amount of specific variation [4]. For example, despite their strong positive correlation, fluid and crystallized intelligence show distinct patterns of age-related decline, and have different responses to working memory training [38], suggesting that their biological bases may substantially overlap but also have unique components. Therefore, our analysis of fluid intelligence targets a specialized domain of cognitive ability, but also contributes to the understanding of the biology of general intelligence.

In addition to the well-replicated finding that higher human intelligence is associated with larger brain size [9–11, 39] and global indices of gray matter volumes [12, 16], several previous studies also investigated regional volumetric and morphological correlates of intelligence. Higher intelligence scores have been associated with increased gray matter volumes across the brain including frontal, temporal, parietal and subcortical regions (e.g., hippocampus) [13–15, 17]. Cortical thickness analyses also reported heterogeneous locations and strengths of associations but positive correlations were consistently observed in the frontal and temporal cortices [18–21]. In this study, we examined the correlations between fluid intelligence and vertex-wise cortical thickness measurements, adjusting for the effect of age and sex, in a much larger sample than previous neuroimaging studies of intelligence. Our results were in line with the literature in the sense that we observed largely bilaterally symmetric associations between fluid intelligence and cortical thickness in several multimodal association regions, including inferior frontal gyrus, superior temporal cortex and proximal regions. That said, we did observe weak positive correlations in the somatomotor cortex and negative correlations in the occipital cortex, which, to our knowledge, has not been reported before.

A major contribution of this study is that we developed a novel statistical method to examine the shared

genetic basis between fluid intelligence and brain morphology at high spatial resolution. Prior studies along this line used the twin design and largely focused on global brain volumes [24–27]. Existing methods for co-heritability and genetic correlation analyses in unrelated individuals either require individual genotypes (e.g., GCTA or GREML) [32] or GWAS summary statistics (e.g., LD score regression) [33] for both traits, which become challenging to apply in high-dimensional settings. We filled this technical gap by formulating co-heritability estimation as a polygenic score analysis. More specifically, the summary statistics of the fluid intelligence GWAS were used to weight individual genotypes of the imaging sample and calculate an individual-specific polygenic score. The polygenic score was then correlated with the cortical thickness measurement at each cortical location and properly scaled to produce a co-heritability estimate. Our method is thus highly computationally efficient and can be applied to estimate the co-heritability between any trait (e.g., a cognitive, behavioral or disease phenotype) whose GWAS summary statistics are available, and a high-dimensional phenotype, such as the MRI-derived vertex-wise cortical thickness measurements in the present study. Permutation procedures can also be devised to enable flexible statistical inferences, such as the cluster-wise analysis [40, 41] on the surface map of co-heritability. Our vertex-wise analysis localized a common genetic basis between fluid intelligence and cortical thickness in predominately left inferior precentral gyrus, pars opercularis, superior temporal cortex, supramarginal gyrus, and their adjacent regions. Intriguingly, some of these regions overlap with Broca's and Wernicke's areas, suggesting that fluid intelligence may have common genetic origins with language-related brain regions. In fact, although fluid intelligence usually does not emphasize the verbal component of human intelligence, the UK Biobank fluid intelligence test requires reading comprehension and verbal reasoning, in addition to inductive and deductive logic abilities (see Methods). Thus, brain regions involved in comprehension of language may be critical to performance in this particular fluid intelligence test. The left precentral gyrus (primary motor cortex) and its vicinity have been found to be consistently activated during reasoning tasks [42, 43], and implicated in lesion mapping of intelligence [44, 45]. Therefore, our results also suggest that fluid intelligence may have a shared genetic basis with brain regions involved in motor processes.

Findings in this analysis should be generalized with caution to populations with different sample characteristics with respect to age range, sex composition, ancestry groups, socioeconomic status, educational attainment or other environmental exposures [38]. Both human intelligence and the cortex undergo rapid development in childhood and adolescence, and age-related decline and degeneration in late adulthood. More importantly, a number of studies have found that the relationship between intelligence and brain morphology is dynamic over time and sex-dependent [see e.g., 39, 46–49]. In this study, we controlled for age, sex, age^2,

age×sex, age^2×sex in all the analyses to remove the (potentially nonlinear) effect of age and sex on intelligence, brain structure, and their correlations. However, since the UK Biobank only recruited middle- and older-aged participants, our results may not be generalizable to other age ranges. In addition, intelligence and genetic influences on intelligence may be moderated by educational opportunities and socioeconomic status (SES) [50–52]. Therefore, our findings should be interpreted in light of the fact that UK Biobank participants are on average more educated and have higher SES than the general population [53].

Although we identified phenotypic and genetic correlations between fluid intelligence and cortical thickness measurements in several brain regions, these correlations do not necessarily indicate causal relationships. Future work using methods such as Mendelian Randomization may shed light on whether genetic influences on human intelligence are mediated through brain morphology. Also, genetic correlation is a genome-wide metric and does not provide any information about specific genes that might underlie both intelligence and brain structure. Further statistical and molecular genetic analyses are needed to dissect their genetic overlap. Lastly, in addition to gray matter volumes and cortical thickness, white matter volumes, diffusion tensor imaging (DTI) derived measurements, functional MRI task activations, and indices of complex brain networks have also been associated with intelligence measurements [4, 8]. Given that a range of features derived from brain morphology, resting state networks, and the structural and functional connectomes are substantially heritable [54–59], integration of multimodal imaging data might provide further insights into possible neural mechanisms of human intelligence.

Methods

The UK Biobank. UK Biobank is a prospective cohort study of 500,000 individuals (age 40-69 years) recruited across Great Britain during 2006-2010 [28]. The protocol and consent were approved by the UK Biobank's Research Ethics Committee. Details about the UK Biobank project are provided at `http://www.ukbiobank.ac.uk`. Data for the current analyses were obtained under an approved data request (ref: 32568; previously 13905).

Genetic data. The genetic data for the UK Biobank comprised 488,377 samples. Two closely related Affymetrix arrays were used to genotype ∼800,000 markers spanning the genome. In addition, the dataset was phased and imputed to ∼96 million variants with the Haplotype Reference Consortium (HRC) [60] and UK10K haplotype resource. We constrained all analyses to the HRC panel in the present study, which com-

bined whole-genome sequence data from multiple cohorts of predominantly European ancestry, and thus covers a large majority of the common genetic variants in the European population.

The genetic data was quality controlled (QC) by the UK Biobank. Important information such as population structure and relatedness has been released. Details about the QC procedures can be found in Bycroft et al. [61]. We leveraged the QC metrics provided by the UK Biobank and removed samples that had mismatch between genetically inferred sex and self-reported sex, high genotype missingness or extreme heterozygosity, sex chromosome aneuploidy, and samples that were excluded from kinship inference and autosomal phasing. We removed one individual from each pair of the samples that were 3rd degree or more closely related relatives, and restricted our analysis to participants that were estimated to have white British ancestry using principal component analysis (PCA).

Brain imaging. We used the T1 structural brain MRI scans from 10,102 participants released by the UK Biobank in February 2017. FreeSurfer [62] version 6.0 was used to process the MRI scans. All processed images were manually inspected and those with processing errors, motion artifacts, poor resolution, pathologies (e.g., tumors) and other abnormalities were removed. Among the 9,229 participants that passed imaging QC, a subset of 7,818 unrelated white British participants additionally passed the genetic QC described above and were included in the analysis. We resampled subject-specific cortical thickness measurements onto FreeSurfer's *fsaverage* representation, which consists of 163,842 vertices per hemisphere with an inter-vertex distance of approximately 1-mm. We further smoothed the co-registered surface maps using a Gaussian kernel with 20-mm full width at half maximum (FWHM).

Fluid intelligence score. The fluid intelligence score (UK Biobank field ID: 20016) used in the present study is an unweighted sum of the number of correct answers given to the 13 fluid intelligence questions as part of the UK Biobank touch-screen questionnaire (`http://biobank.ctsu.ox.ac.uk/crystal/refer.cgi?id=100231`). Participants who did not answer all of the questions within the allotted 2-minute limit were scored as zero for each of the unattempted questions. The score is roughly normal distributed (Supplementary Figure S4) and was thus treated as a quantitative variable in this study. Of all the participants that passed genetic QC, 108,147 (age, 40-70 y; female, 53.51%) had fluid intelligence scores at the baseline assessment visit (2006–2010) and were used in the fluid intelligence GWAS. Of the 7,818 participants (age, 45-79 y; female, 52.24%) that passed both imaging and genetic QC, 7,485 (age, 45-79 y; female, 52.22%) additionally had fluid intelligence scores at the imaging visit (after 2014), and were used in assessing the phenotypic correlations between fluid intelligence and cortical thickness measurements. There was no overlap

between the fluid intelligence GWAS sample and the neuroimaging sample.

GWAS of fluid intelligence. We performed GWAS of the fluid intelligence score in 108,147 participants. In addition to the genetic sample QC described above, we filtered out genetic markers with minor allele frequency $< 1\%$ and imputation quality score < 0.8. A total of 7,658,275 imputed SNPs on the HRC panel were included in the GWAS. Association tests were conducted using SNPTEST v2.5.2 [63]. For each genetic marker, a linear regression model was fitted, adjusting for age (at the baseline assessment visit), sex, age^2, age$\times$sex, age$^2\times$sex, genotype array, UK Biobank assessment center, and top 10 PCs of the genotype data as covariates. GWAS results were visualized using the platform FUMA [64].

Phenotypic correlation. Pearson correlations between the fluid intelligence score collected at the imaging visit and vertex-wise cortical thickness measurements were computed using data from 7,485 participants, adjusting for age (at the imaging visit), sex, age^2, age$\times$sex, age$^2\times$sex as covariates.

Estimators for SNP heritability. Consider the linear model $\boldsymbol{y} = \boldsymbol{X}\boldsymbol{\beta} + \boldsymbol{\epsilon}$, where $\boldsymbol{y}$ is an $N \times 1$ vector of covariate-adjusted and standardized phenotypes, $\boldsymbol{X} = [x_{ij}]_{N\times M}$ is an $N \times M$ matrix of genotypes with each column $\boldsymbol{x}_j$ normalized to mean zero and variance one, $\boldsymbol{\beta}$ is an $M \times 1$ vector of (random) SNP effect sizes, and $\boldsymbol{\epsilon}$ is an $N \times 1$ vector of residuals. In *Supplementary Information*, we show that under a polygenic model, the following moment-matching estimators for SNP heritability are asymptotically equivalent:

$$\widehat{h}^2_{g,\mathrm{LDSC}} = C_{h^2}\left(\overline{\chi}^2 - 1\right), \qquad \widehat{h}^2_{g,\mathrm{HE}} = C_{h^2}\left(\frac{1}{N}\boldsymbol{y}^\top \boldsymbol{K}\boldsymbol{y} - 1\right), \qquad \widehat{h}^2_{g,\mathrm{PS}} = C_{h^2}\big(\langle \boldsymbol{\xi}, \boldsymbol{y}\rangle - 1\big), \tag{1}$$

where $C_{h^2} = \dfrac{M}{\overline{\ell} N} \approx \dfrac{N}{\sum_{i\neq j} k_{ij}^2}$ is a constant, $\boldsymbol{K} = [k_{ij}]_{N\times N} = \boldsymbol{X}\boldsymbol{X}^\top/M$ is the empirical genetic relationship matrix, $\overline{\ell}$ is the average LD score across the genome, $\widehat{\beta}_j = \boldsymbol{x}_j^\top \boldsymbol{y}/N$ is the marginal effect size estimate of the j-th variant with $\widehat{\chi}^2_j = N\widehat{\beta}^2_j$ being the corresponding χ^2 statistic, $\overline{\chi}^2$ is the average χ^2 statistic across the genome, $\boldsymbol{\xi} = \dfrac{1}{M}\sum_{j=1}^{M} \boldsymbol{x}_j \widehat{\beta}_j$ is a weighted average of the genotype, i.e., an $N \times 1$ vector of individual-specific polygenic scores, and $\langle \cdot, \cdot \rangle$ denotes inner product, i.e., $\langle \boldsymbol{\xi}, \boldsymbol{y}\rangle = \boldsymbol{\xi}^\top \boldsymbol{y}$.

We note that $\widehat{h}^2_{g,\mathrm{LDSC}}$ is the LD score regression estimator based on GWAS summary statistics, with the intercept constrained to one and the reciprocal of the LD score as the regression weight [34]. $\widehat{h}^2_{g,\mathrm{HE}}$ is the Haseman-Elston regression estimator based on individual genotypes [35, 65–67]. $\widehat{h}^2_{g,\mathrm{PS}}$ formulates SNP heritability estimation as a polygenic score analysis. The equivalence between $\widehat{h}^2_{g,\mathrm{LDSC}}$ and $\widehat{h}^2_{g,\mathrm{HE}}$ has been established both theoretically and empirically in prior work [35, 68, 69].

Estimators for SNP co-heritability. Consider the bivariate model $\boldsymbol{y}_1 = \boldsymbol{X}_1\boldsymbol{\beta}_1 + \boldsymbol{\epsilon}_1$ and $\boldsymbol{y}_2 = \boldsymbol{X}_2\boldsymbol{\beta}_2 + \boldsymbol{\epsilon}_2$, where $\boldsymbol{y}_1$ and $\boldsymbol{y}_2$ are $N_1 \times 1$ and $N_2 \times 1$ vectors of covariate-adjusted and standardized phenotypes, $\boldsymbol{X}_1$ and $\boldsymbol{X}_2$ are $N_1 \times M$ and $N_2 \times M$ matrices of standardized genotypes, $\boldsymbol{\beta}_1$ and $\boldsymbol{\beta}_2$ are $M \times 1$ vectors of SNP effect sizes, $\boldsymbol{\epsilon}_1$ and $\boldsymbol{\epsilon}_2$ are $N_1 \times 1$ and $N_2 \times 1$ vectors of residuals, respectively. Without loss of generality, we assume that the first N_s samples are identical for the two phenotypes. In *Supplementary Information*, we show that under a polygenic model, the following moment-matching estimators for SNP co-heritability are asymptotically equivalent:

$$\begin{aligned} \widehat{\rho}_{g,\mathrm{LDSC}} &= C_{\rho_g}\left(\overline{z_1 z_2} - \frac{N_s\rho}{\sqrt{N_1 N_2}}\right), \qquad \widehat{\rho}_{g,\mathrm{HE}} = C_{\rho_g}\left(\frac{1}{\sqrt{N_1 N_2}}\boldsymbol{y}_1^\top \boldsymbol{K}_c \boldsymbol{y}_2 - \frac{N_s\rho}{\sqrt{N_1 N_2}}\right), \\ \widehat{\rho}_{g,\mathrm{PS}} &= C_{\rho_g}\left(\sqrt{\frac{N_2}{N_1}}\langle\boldsymbol{\xi}_1, \boldsymbol{y}_1\rangle - \frac{N_s\rho}{\sqrt{N_1 N_2}}\right) = C_{\rho_g}\left(\sqrt{\frac{N_1}{N_2}}\langle\boldsymbol{\xi}_2, \boldsymbol{y}_2\rangle - \frac{N_s\rho}{\sqrt{N_1 N_2}}\right), \end{aligned} \tag{2}$$

where $C_{\rho_g} = \dfrac{M}{\ell\sqrt{N_1 N_2}} \approx \dfrac{\sqrt{N_1 N_2}}{\sum_{(i,j)\notin\mathcal{I}} k_{c,ij}^2}$ is a constant, $\mathcal{I} = \{(i,j) \mid 1 \leqslant i = j \leqslant N_s\}$, $\boldsymbol{K}_c = [k_{c,ij}]_{N_1\times N_2} = \boldsymbol{X}_1\boldsymbol{X}_2^\top/M$, ρ is the phenotypic correlation between the two traits, $\widehat{\beta}_{1j} = \boldsymbol{x}_{1j}^\top\boldsymbol{y}_1/N_1$ and $\widehat{\beta}_{2j} = \boldsymbol{x}_{2j}^\top\boldsymbol{y}_2/N_2$ are marginal effect size estimates of the j-th variant, with $\widehat{z}_{1j} = \boldsymbol{x}_{1j}^\top\boldsymbol{y}_1/\sqrt{N_1}$ and $\widehat{z}_{2j} = \boldsymbol{x}_{2j}^\top\boldsymbol{y}_2/\sqrt{N_2}$ being the corresponding z statistics, respectively, $\overline{z_1 z_2} = \dfrac{1}{M}\sum_{j=1}^{M}\widehat{z}_{1j}\widehat{z}_{2j}$ is the average product of z statistics across the genome, $\boldsymbol{\xi}_1 = \dfrac{1}{M}\sum_{j=1}^{M}\boldsymbol{x}_{1j}\widehat{\beta}_{2j}$ and $\boldsymbol{\xi}_2 = \dfrac{1}{M}\sum_{j=1}^{M}\boldsymbol{x}_{2j}\widehat{\beta}_{1j}$ are individual-specific polygenic scores.

We note that $\widehat{\rho}_{g,\mathrm{LDSC}}$ is the LD score regression estimator based on GWAS summary statistics, with constrained intercept and the reciprocal of the LD score as the regression weight [33]. $\widehat{\rho}_{g,\mathrm{HE}}$ is the Haseman-Elston regression estimator based on individual genotypes. $\widehat{\rho}_{g,\mathrm{PS}}$ formulates SNP co-heritability estimation as a polygenic score analysis, and thus enables co-heritability analysis when GWAS summary statistics are available for one trait and individual genotypes are available for the other trait. The equivalence between $\widehat{\rho}_{g,\mathrm{LDSC}}$ and $\widehat{\rho}_{g,\mathrm{HE}}$ has been established in prior work [68].

Statistical genetic analyses. For all heritability and co-heritability analyses, we used SNPs in the HapMap3 panel whose LD scores have been computed and released (https://github.com/bulik/ldsc). We further filtered out genetic markers with imputation quality score < 0.9, missing rate $> 1\%$, minor allele frequency $< 1\%$, and significant deviation from Hardy-Weinberg equilibrium ($p < 1 \times 10^{-10}$) in the UK Biobank. A total of 871,023 SNPs were used in heritability and co-heritability analyses.

The SNP heritability of the fluid intelligence score, denoted as $\widehat{h}^2_{\mathrm{Gf}}$, was computed using the LD score regression estimator $\widehat{h}^2_{g,\mathrm{LDSC}}$ in Eq. (1) and the summary statistics of the fluid intelligence GWAS in the UK

Biobank ($N = 108,147$). The SNP heritability of the cortical thickness measurement at vertex v, denoted as $\widehat{h}^2_v$, was computed using the Haseman-Elston regression estimator $\widehat{h}^2_{g,\mathrm{HE}}$ in Eq. (1) and individual genotypes of the imaging sample ($N = 7,818$). We adjusted for age (at the imaging visit), sex, age^2, age$\times$sex, age$^2\times$sex, genotype array, and top 10 PCs of the genotype data as covariates. Vertex-wise estimates $\widehat{h}^2_v$, $v = 1, 2, \cdots, V$, where V is the total number of vertices, form a surface map for the heritability of cortical thickness measurements.

The SNP co-heritability between the fluid intelligence score and the cortical thickness measurement at vertex v, denoted as $\widehat{\rho}_{\mathrm{Gf},v}$, was computed using the estimator $\widehat{\rho}_{g,\mathrm{PS}}$ in Eq. (2). More specifically, the summary statistics of the fluid intelligence GWAS ($N = 108,147$) were used to calculate an individual-specific polygenic score in the imaging sample ($N = 7,818$) where individual genotypes were available. The polygenic score was then correlated with the cortical thickness measurement at each cortical location and properly scaled to produce the co-heritability estimate. Since there was no overlap between the fluid intelligence GWAS sample and neuroimaging sample, the bias term in the estimator, i.e., $N_s\rho/\sqrt{N_1N_2}$, was set to zero. We adjusted for age (at the imaging visit), sex, age^2, age$\times$sex, age$^2\times$sex, genotype array, and top 10 PCs of the genotype data as covariates in the co-heritability (polygenic score) analysis.

Vertex-wise estimates $\widehat{\rho}_{\mathrm{Gf},v}$, $v = 1, 2, \cdots, V$, form a surface map for the co-heritability between fluid intelligence and cortical thickness measurements. Clusters on the surface map can be defined by spatially contiguous vertices with co-heritability estimates above a predefined threshold (or equivalently, p-values below a threshold). To assess the significance of the size (number of vertices) of a cluster while accounting for the spatial correlation of cortical thickness measurements, we employed the following permutation procedure. For each permutation $k = 1, 2, \cdots, N_{\mathrm{perm}}$, we recomputed and thresholded the co-heritability map using a permuted polygenic score, and recorded the maximal cluster size M_k across the two hemispheres. Then for an observed cluster $\mathcal{C}$ with size c, the family-wise error (FWE) corrected p-value is [70]

$$p_{\mathrm{FWE}}(\mathcal{C}) = \frac{\#\{M_k \geqslant c\}}{N_{\mathrm{perm}}}. \tag{3}$$

Genetic correlation between the fluid intelligence score and cortical thickness measurement at each vertex was computed as

$$\widehat{r}_{\mathrm{Gf},v} = \frac{\widehat{\rho}_{\mathrm{Gf},v}}{\sqrt{\widehat{h}^2_{\mathrm{Gf}}\widehat{h}^2_v}}, \qquad v = 1, 2, \cdots, V. \tag{4}$$

Acknowledgements

This research was carried out in part at the Athinoula A. Martinos Center for Biomedical Imaging at the Massachusetts General Hospital (MGH), using resources provided by the Center for Functional Neuroimaging Technologies, P41EB015896, a P41 Biotechnology Resource Grant supported by the National Institute of Biomedical Imaging and Bioengineering (NIBIB), National Institutes of Health (NIH). This work involved the use of instrumentation supported by the NIH Shared Instrumentation Grant Program; specifically, grant numbers S10RR023043 and S10RR023401. This research was also funded in part by NIH grants K99AG054573 (TG); R01MH095904 and R01MH109562 (DJH); R01AG053949 and R01LM012719 (MRS); and K24MH094614 (JWS). JWS is a Tepper Family MGH Research Scholar and was also supported in part by a gift from the Demarest Lloyd, Jr. Foundation. The funders had no role in study design, data collection and analysis, decision to publish, or preparation of the manuscript. This research has been conducted using the UK Biobank resource under an approved data request (ref: 32568; previously 13905).

References

[1] J.B. Carroll. *Human cognitive abilities: A survey of factor-analytic studies*. Cambridge University Press, 1993.

[2] I.J. Deary. Intelligence. *Annual Review of Psychology*, 63:453–482, 2012.

[3] K.M. Keyes, J. Platt, A.S. Kaufman, and K.A. McLaughlin. Association of fluid intelligence and psychiatric disorders in a population-representative sample of US adolescents. *JAMA Psychiatry*, 74(2): 179–188, 2017.

[4] I.J. Deary, L. Penke, and W. Johnson. The neuroscience of human intelligence differences. *Nature Reviews Neuroscience*, 11(3):201–211, 2010.

[5] T.J.C. Polderman, B. Benyamin, C.A. De Leeuw, P.F. Sullivan, A. Van Bochoven, et al. Meta-analysis of the heritability of human traits based on fifty years of twin studies. *Nature Genetics*, 47(7):702–709, 2015.

[6] S. Sniekers, S. Stringer, K. Watanabe, P.R. Jansen, J.R.I. Coleman, et al. Genome-wide association

meta-analysis of 78,308 individuals identifies new loci and genes influencing human intelligence. *Nature Genetics*, 49(7):1107–1112, 2017.

[7] J.E. Savage, P.R. Jansen, S. Stringer, K. Watanabe, J. Bryois, et al. GWAS meta-analysis (N=279,930) identifies new genes and functional links to intelligence. *bioRxiv*, 184853, 2017.

[8] E. Luders, K.L. Narr, P.M. Thompson, and A.W. Toga. Neuroanatomical correlates of intelligence. *Intelligence*, 37(2):156–163, 2009.

[9] J.P. Rushton and C.D. Ankney. Whole brain size and general mental ability: a review. *International Journal of Neuroscience*, 119(5):692–732, 2009.

[10] M.A. McDaniel. Big-brained people are smarter: A meta-analysis of the relationship between in vivo brain volume and intelligence. *Intelligence*, 33(4):337–346, 2005.

[11] J.C. Wickett, P.A. Vernon, and D.H. Lee. Relationships between factors of intelligence and brain volume. *Personality and Individual Differences*, 29(6):1095–1122, 2000.

[12] N.C. Andreasen, M. Flaum, V. Swayze 2nd, D.S. O'Leary, R. Alliger, et al. Intelligence and brain structure in normal individuals. *The American Journal of Psychiatry*, 150(1):130, 1993.

[13] L.A. Flashman, N.C. Andreasen, M. Flaum, and V.W. Swayze. Intelligence and regional brain volumes in normal controls. *Intelligence*, 25(3):149–160, 1997.

[14] A.M.J. MacLullich, K.J. Ferguson, I.J. Deary, J.R. Seckl, J.M. Starr, et al. Intracranial capacity and brain volumes are associated with cognition in healthy elderly men. *Neurology*, 59(2):169–174, 2002.

[15] R.J. Haier, R. Colom, D.H. Schroeder, C.A. Condon, C. Tang, et al. Gray matter and intelligence factors: Is there a neuro-g? *Intelligence*, 37(2):136–144, 2009.

[16] R. Colom, R.E. Jung, and R.J. Haier. Distributed brain sites for the g-factor of intelligence. *NeuroImage*, 31(3):1359–1365, 2006.

[17] R.J. Haier, R.E. Jung, R.A. Yeo, K. Head, and M.T. Alkire. Structural brain variation and general intelligence. *NeuroImage*, 23(1):425–433, 2004.

[18] K.L. Narr, R.P. Woods, P.M. Thompson, P. Szeszko, D. Robinson, et al. Relationships between IQ and regional cortical gray matter thickness in healthy adults. *Cerebral Cortex*, 17(9):2163–2171, 2007.

[19] Y.Y. Choi, N.A. Shamosh, S.H. Cho, C.G. DeYoung, M.J. Lee, , et al. Multiple bases of human intelligence revealed by cortical thickness and neural activation. *Journal of Neuroscience*, 28(41):10323–10329, 2008.

[20] S. Karama, Y. Ad-Dab'bagh, R.J. Haier, I.J. Deary, O.C. Lyttelton, et al. Positive association between cognitive ability and cortical thickness in a representative US sample of healthy 6 to 18 year-olds. *Intelligence*, 37:145–155, 2009.

[21] K. Menary, P.F. Collins, J.N. Porter, R. Muetzel, E.A. Olson, et al. Associations between cortical thickness and general intelligence in children, adolescents and young adults. *Intelligence*, 41(5):597–606, 2013.

[22] R.E. Jung and R.J. Haier. The Parieto-Frontal Integration Theory (P-FIT) of intelligence: converging neuroimaging evidence. *Behavioral and Brain Sciences*, 30(2):135–154, 2007.

[23] R. Colom, R.J. Haier, K. Head, J. Álvarez-Linera, M.Á. Quiroga, et al. Gray matter correlates of fluid, crystallized, and spatial intelligence: Testing the P-FIT model. *Intelligence*, 37(2):124–135, 2009.

[24] P.M. Thompson, T.D. Cannon, K.L. Narr, T. Van Erp, V.P. Poutanen, et al. Genetic influences on brain structure. *Nature Neuroscience*, 4(12):1253–1258, 2001.

[25] D. Posthuma, E.J.C. De Geus, W.F.C. Baaré, H.E.H. Pol, R.S. Kahn, et al. The association between brain volume and intelligence is of genetic origin. *Nature Neuroscience*, 5(2):83–84, 2002.

[26] D. Posthuma, W.F.C. Baaré, H.E.H. Pol, R.S. Kahn, D.I. Boomsma, et al. Genetic correlations between brain volumes and the WAIS-III dimensions of verbal comprehension, working memory, perceptual organization, and processing speed. *Twin Research and Human Genetics*, 6(2):131–139, 2003.

[27] H.E.H. Pol, H.G. Schnack, D. Posthuma, R.C.W. Mandl, W.F. Baaré, et al. Genetic contributions to human brain morphology and intelligence. *Journal of Neuroscience*, 26(40):10235–10242, 2006.

[28] C. Sudlow, J. Gallacher, N. Allen, V. Beral, P. Burton, et al. UK biobank: an open access resource for identifying the causes of a wide range of complex diseases of middle and old age. *PLoS Medicine*, 12 (3):e1001779, 2015.

[29] R.B. Cattell. *Abilities: Their structure, growth, and action*. Houghton Mifflin, 1971.

[30] C. Spearman. "general Intelligence," objectively determined and measured. *The American Journal of Psychology*, 15(2):201–292, 1904.

[31] W. Johnson, T.J. Bouchard, R.F. Krueger, M. McGue, and I.I. Gottesman. Just one g: Consistent results from three test batteries. *Intelligence*, 32(1):95–107, 2004.

[32] J. Yang, S.H. Lee, M.E. Goddard, and P.M. Visscher. GCTA: a tool for genome-wide complex trait analysis. *The American Journal of Human Genetics*, 88(1):76–82, 2011.

[33] B. Bulik-Sullivan, H.K. Finucane, V. Anttila, A. Gusev, F.R. Day, et al. An atlas of genetic correlations across human diseases and traits. *Nature Genetics*, 47(11):1236–1241, 2015.

[34] B.K. Bulik-Sullivan, P. Loh, H.K. Finucane, S. Ripke, J. Yang, et al. LD score regression distinguishes confounding from polygenicity in genome-wide association studies. *Nature Genetics*, 47(3):291–295, 2015.

[35] T. Ge, C.Y. Chen, B.M. Neale, M.R. Sabuncu, and J.W. Smoller. Phenome-wide heritability analysis of the UK Biobank. *PLoS Genetics*, 13(4):e1006711, 2017.

[36] R.S. Desikan, F. Ségonne, B. Fischl, B.T. Quinn, B.C. Dickerson, et al. An automated labeling system for subdividing the human cerebral cortex on MRI scans into gyral based regions of interest. *NeuroImage*, 31(3):968–980, 2006.

[37] G. Davies, A. Tenesa, A. Payton, J. Yang, S.E. Harris, et al. Genome-wide association studies establish that human intelligence is highly heritable and polygenic. *Molecular Psychiatry*, 16(10):996–1005, 2011.

[38] R.E. Nisbett, J. Aronson, C. Blair, W. Dickens, J. Flynn, et al. Intelligence: new findings and theoretical developments. *American Psychologist*, 67(2):130, 2012.

[39] S.F. Witelson, H. Beresh, and D.L. Kigar. Intelligence and brain size in 100 postmortem brains: sex, lateralization and age factors. *Brain*, 129(2):386–398, 2006.

[40] K.J. Friston, K.J. Worsley, R.S.J. Frackowiak, J.C. Mazziotta, and A.C. Evans. Assessing the significance of focal activations using their spatial extent. *Human Brain Mapping*, 1(3):210–220, 1994.

[41] K.J. Friston, A. Holmes, J.B. Poline, C.J. Price, and C.D. Frith. Detecting activations in PET and fMRI: levels of inference and power. *NeuroImage*, 4(3):223–235, 1996.

[42] J. Prado, A. Chadha, and J.R. Booth. The brain network for deductive reasoning: a quantitative meta-analysis of 28 neuroimaging studies. *Journal of Cognitive Neuroscience*, 23(11):3483–3497, 2011.

[43] B.D. Acuna, J.C. Eliassen, J.P. Donoghue, and J.N. Sanes. Frontal and parietal lobe activation during transitive inference in humans. *Cerebral Cortex*, 12(12):1312–1321, 2002.

[44] J. Gläscher, D. Rudrauf, R. Colom, L.K. Paul, D. Tranel, et al. Distributed neural system for general intelligence revealed by lesion mapping. *Proceedings of the National Academy of Sciences*, 107(10): 4705–4709, 2010.

[45] A. Woolgar, A. Parr, R. Cusack, R. Thompson, I. Nimmo-Smith, et al. Fluid intelligence loss linked to restricted regions of damage within frontal and parietal cortex. *Proceedings of the National Academy of Sciences*, 107(33):14899–14902, 2010.

[46] P. Shaw, D. Greenstein, J. Lerch, L. Clasen, R. Lenroot, et al. Intellectual ability and cortical development in children and adolescents. *Nature*, 440(7084):676–679, 2006.

[47] A.L. Reiss, M.T. Abrams, H.S. Singer, J.L. Ross, and M.B. Denckla. Brain development, gender and IQ in children: a volumetric imaging study. *Brain*, 119(5):1763–1774, 1996.

[48] R.C. Gur, B.I. Turetsky, M. Matsui, M. Yan, W. Bilker, et al. Sex differences in brain gray and white matter in healthy young adults: correlations with cognitive performance. *Journal of Neuroscience*, 19 (10):4065–4072, 1999.

[49] M. Burgaleta, W. Johnson, D.P. Waber, R. Colom, and S. Karama. Cognitive ability changes and dynamics of cortical thickness development in healthy children and adolescents. *NeuroImage*, 84:810–819, 2014.

[50] I.J. Deary and W. Johnson. Intelligence and education: causal perceptions drive analytic processes and therefore conclusions. *International Journal of Epidemiology*, 39(5):1362–1369, 2010.

[51] S. Von Stumm and R. Plomin. Socioeconomic status and the growth of intelligence from infancy through adolescence. *Intelligence*, 48:30–36, 2015.

[52] K.B. Hanscombe, M. Trzaskowski, C.M.A. Haworth, O.S.P. Davis, P.S. Dale, et al. Socioeconomic status (SES) and children's intelligence (IQ): In a UK-representative sample SES moderates the environmental, not genetic, effect on IQ. *PLoS One*, 7(2):e30320, 2012.

[53] J. Tyrrell, S.E. Jones, R. Beaumont, C.M. Astley, R. Lovell, et al. Height, body mass index, and socioeconomic status: mendelian randomisation study in UK biobank. *BMJ*, 352:i582, 2016.

[54] T. Ge, T.E. Nichols, P.H. Lee, A.J. Holmes, J.L. Roffman, et al. Massively expedited genome-wide heritability analysis (MEGHA). *Proceedings of the National Academy of Sciences*, 112(8):2479–2484, 2015.

[55] T. Ge, M. Reuter, A.M. Winkler, A.J. Holmes, P.H. Lee, et al. Multidimensional heritability analysis of neuroanatomical shape. *Nature Communications*, 7:13291, 2016.

[56] T. Ge, A.J. Holmes, R.L. Buckner, J.W. Smoller, and M.R. Sabuncu. Heritability analysis with repeat measurements and its application to resting-state functional connectivity. *Proceedings of the National Academy of Sciences*, 114(21):5521–5526, 2017.

[57] D.C. Glahn, A.M. Winkler, P. Kochunov, L. Almasy, R. Duggirala, et al. Genetic control over the resting brain. *Proceedings of the National Academy of Sciences*, 107(3):1223–1228, 2010.

[58] P.M. Thompson, T. Ge, D.C. Glahn, N. Jahanshad, and T.E. Nichols. Genetics of the connectome. *NeuroImage*, 80:475–488, 2013.

[59] P. Kochunov, N. Jahanshad, D. Marcus, A. Winkler, E. Sprooten, et al. Heritability of fractional anisotropy in human white matter: a comparison of Human Connectome Project and ENIGMA-DTI data. *NeuroImage*, 111:300–311, 2015.

[60] Haplotype Reference Consortium. A reference panel of 64,976 haplotypes for genotype imputation. *Nature Genetics*, 48(10):1279–1283, 2016.

[61] C. Bycroft, C. Freeman, D. Petkova, G. Band, L.T. Elliott, et al. Genome-wide genetic data on ~500,000 UK Biobank participants. *bioRxiv*, 166298, 2017.

[62] B. Fischl. Freesurfer. *NeuroImage*, 62(2):774–781, 2012.

[63] J. Marchini and B. Howie. Genotype imputation for genome-wide association studies. *Nature Reviews Genetics*, 11(7):499–511, 2010.

[64] K. Watanabe, E. Taskesen, A. van Bochoven, and D. Posthuma. FUMA: Functional mapping and annotation of genetic associations. *Nature Communications*, 8:1826, 2017.

[65] J.K. Haseman and R.C. Elston. The investigation of linkage between a quantitative trait and a marker locus. *Behavior Genetics*, 2(1):3–19, 1972.

[66] R.C. Elston, S. Buxbaum, K.B. Jacobs, and J.M. Olson. Haseman and Elston revisited. *Genetic Epidemiology*, 19(1):1–17, 2000.

[67] D. Golan, E.S. Lander, and S. Rosset. Measuring missing heritability: inferring the contribution of common variants. *Proceedings of the National Academy of Sciences*, 111(49):E5272–E5281, 2014.

[68] B. Bulik-Sullivan. Relationship between LD score and Haseman-Elston regression. *bioRxiv*, 018283, 2015.

[69] X. Zhou. A unified framework for variance component estimation with summary statistics in genome-wide association studies. *The Annals of Applied Statistics*, 11(4):2027–2051, 2017.

[70] P.H. Westfall and S.S. Young. *Resampling-based multiple testing: Examples and methods for p-value adjustment*. John Wiley & Sons, 1993.